Magnetic Casimir effect

G. Metalidis and P. Bruno*
Max-Planck-Institut für Mikrostrukturphysik, Weinberg 2, D-06120 Halle, Germany†
(Received 26 July 2002; published 5 December 2002)

The Casimir effect results from alterations of the zero-point electromagnetic energy introduced by boundary conditions. For ferromagnetic layers separated by vacuum (or a dielectric), such boundary conditions are influenced by the magneto-optical Kerr effect. We will show that this gives rise to a long-range magnetic interaction and discuss the effect for two different configurations (magnetization parallel and perpendicular to the layers). Analytical expressions are derived for two models and compared to numerical calculations. Numerical calculations of the effect for Fe are also presented and the possibility of an experimental observation of the Casimir magnetic interaction is discussed.

DOI: 10.1103/PhysRevA.66.062102 PACS number(s): 12.20.Ds, 03.70.+k, 12.90.+b, 78.20.Ls

I. INTRODUCTION

Since its discovery, the Casimir effect has gradually become a much-discussed subject in physics. Originally, one understood by the Casimir effect the attractive force between two metal plates in vacuum as a result of zero-point quantum fluctuations [1]. Nowadays the term is used for a much broader range of effects, all involving the influence of boundaries on fluctuations. As such, the Casimir effect plays a role in quantum-field theory, atomic and molecular physics, condensed-matter physics, gravitation, cosmology, and so on. A thorough review of the Casimir effect in all these fields was published recently [2].

For two uniformly magnetized ferromagnetic plates held parallel to each other, it is shown in a previous paper [3] that the interplay of the Casimir effect and the magneto-optical Kerr effect gives rise to a new long-range magnetic interaction. In Ref. [3], this magnetic Casimir force was found to decay with interplate distance D as D^{-5} in the limit of long distances, and as D^{-1} for short distances. In this case, the ferromagnetic plates were described with a Drude model and the magnetization was defined to be perpendicular to the plates. In view of future experimental investigations of this new magnetic Casimir force, it would be useful to study the case where the magnetization is parallel to the plates since this situation is easier to obtain in an experimental setup. This subject will be studied in the present paper and a force that decays as D^{-6} in the long-distance limit and as D^{-3} in the limit of short distances is found when the Drude model is used. This behavior is interesting since it means that the force is larger, and thus easier to measure, for in-plane magnetization than for perpendicular magnetization at sufficiently small distances. Next to the Drude model, another more realistic model is also studied. In this so-called hybrid model, a plasma model is used for the diagonal element of the dielectric tensor of the magnetic plates, and a single absorption line model for the off-diagonal element. As for the long-distance limit, the force in this model goes like D^{-8} for the case of perpendicular magnetization and as D^{-10} when the magnetization is parallel to the plates, while the behavior in the short-distance limit is unchanged. Finally, we will present some numerical calculations of the interaction for Fe, in which experimental data for the elements of the dielectric tensor are used. An experimental setup to measure the magnetic Casimir force is also discussed.

II. GENERAL THEORY

Consider two uniformly magnetized ferromagnetic plates of infinite lateral extension held parallel to each other. The Casimir interaction energy per unit area at $T=0$ between the plates can be expressed [4] as

$$\mathcal{E}=\frac{\hbar}{(2\pi)^3}\int_0^{+\infty} d\omega \int d^2\boldsymbol{k}_{\parallel}\,\mathrm{Im\,Tr\,ln}(1-\mathsf{R}_A\mathsf{R}_B e^{2ik_{\perp}D}), \tag{1}$$

where $k_{\perp}$ and $\boldsymbol{k}_{\parallel}$ are the components of the wave vector perpendicular and parallel to the mirrors. The 2×2 matrices R_A and R_B contain the reflection coefficients of the two mirrors:

$$\mathsf{R}_{A(B)}=\begin{pmatrix} r_{ss}^{A(B)} & r_{sp}^{A(B)} \\ r_{ps}^{A(B)} & r_{pp}^{A(B)} \end{pmatrix}. \tag{2}$$

The index s (p) corresponds to a polarization with the electric field perpendicular (parallel) to the incidence plane. We will adopt here the usual convention that the s axis remains unchanged upon reflection. Since the reflection coefficients are dependent on the direction of the magnetization of the mirrors, it is clear from Eqs. (1) and (2) that the magnetic Casimir energy between the mirrors will differ for the situations in which the magnetizations of the two mirrors are parallel [ferromagnetic (FM)] or antiparallel [antiferromagnetic (AF)]. This will result in a net magnetic Casimir force per unit area $\Delta\mathcal{F}\equiv\mathcal{F}_{AF}-\mathcal{F}_{FM}$ between the mirrors, different from the ordinary Casimir force discussed in Ref. [1].

If a change of integration variables $(\omega,\boldsymbol{k}_{\parallel})\rightarrow(\omega,k_{\perp},\varphi)$ is performed and complex integration methods are used as in Ref. [4], Eq. (1) can be written as

*Electronic address: bruno@mpi-halle.de
†URL: http://www.mpi-halle.de

$$\mathcal{E}=\frac{\hbar}{(2\pi)^3}\int_0^{+\infty}dk_\perp k_\perp\int_0^{2\pi}d\varphi\int_0^{k_\perp c}d\omega\,\mathrm{Re\,Tr\,ln}[1-\mathsf{R}_A(i\omega,ik_\perp,\varphi)\mathsf{R}_B(i\omega,ik_\perp,\varphi)e^{-2k_\perp D}]. \tag{3}$$

In general, the reflection coefficients contain terms of different orders of the magneto-optical constant Q. In our calculation, only terms up to first order in Q will be conserved. When the magnetization direction is reversed, these terms will change sign. Since the first-order terms are usually much smaller than 1, and than the terms that are independent of Q, it is possible to expand expression (3) to lowest order in the linear terms.

A. The polar configuration

After some algebra, we find for the situation with magnetization directed perpendicular to the plates (we will call this the polar configuration from now on):

$$\Delta\mathcal{E}^\perp=\mathcal{E}^\perp_{AF}-\mathcal{E}^\perp_{AM}\approx-\frac{\hbar}{\pi^2}\int_0^{+\infty}dk_\perp k_\perp\int_0^{k_\perp c}d\omega\,\mathrm{Re}\left[\frac{(r^\perp_{sp})^2e^{-2k_\perp D}}{(1-r^2_{ss}e^{-2k_\perp D})(1-r^2_{pp}e^{-2k_\perp D})}\right], \tag{4a}$$

$$\Delta\mathcal{F}^\perp=-\frac{\mathrm{d}\Delta\mathcal{E}^\perp}{\mathrm{d}D}\approx-\frac{2\hbar}{\pi^2}\int_0^{+\infty}\mathrm{d}k_\perp k_\perp^2\int_0^{k_\perp c}\mathrm{d}\omega\,\mathrm{Re}\left[\frac{(r^\perp_{sp})^2[1-r^2_{ss}r^2_{pp}\mathrm{e}^{-4k_\perp D}]\mathrm{e}^{-2k_\perp D}}{([1-r^2_{ss}\mathrm{e}^{-2k_\perp D}][1-r^2_{pp}\mathrm{e}^{-2k_\perp D}])^2}\right], \tag{4b}$$

where the reflection coefficients have to be evaluated at imaginary perpendicular wavevector and frequency. In this equation, the reflection amplitudes are supposed to be identical for the two mirrors. Otherwise, the squared reflection coefficients have to be replaced by the product of the coefficients for the separate mirrors (e.g. $r^2_{ss}\to r^A_{ss}r^B_{ss}$). The integral over the angle φ is already performed. The reflection coefficients for a mirror in the polar configuration are given in Ref. [5] as

$$r_{ss}(i\omega,ik_\perp)=\frac{k_\perp c-\xi}{k_\perp c+\xi},\quad r_{pp}(i\omega,ik_\perp)=\frac{\varepsilon_{xx}(i\omega)k_\perp c-\xi}{\varepsilon_{xx}(i\omega)k_\perp c+\xi}, \tag{5a}$$

$$r^\perp_{sp}(i\omega,ik_\perp)=r^\perp_{ps}(i\omega,ik_\perp)=\frac{-k_\perp c\,\omega\,\varepsilon_{xy}(i\omega)}{[k_\perp c+\xi][\varepsilon_{xx}(i\omega)k_\perp c+\xi]}, \tag{5b}$$

with $\xi=\sqrt{\omega^2[\varepsilon_{xx}(i\omega)-1]+(k_\perp c)^2}$.

B. The in-plane configuration

For the case where the magnetization is parallel to the plates (we will refer to this situation as the in-plane configuration from now on), not only r_{sp}, but also r_{pp} will contain a term that is linear in the magneto-optical constant. As a consequence, we find two contributions to the Casimir magnetic interaction energy. The first one ($\Delta\mathcal{E}^\parallel_1$) results from the longitudinal Kerr effect, while the second term ($\Delta\mathcal{E}^\parallel_2$) is a consequence of the transversal Kerr effect. Again the integral over φ can be performed directly. We obtain (for identical mirrors)

$$\Delta\mathcal{E}^\parallel_1\approx\frac{\hbar}{2\pi^2}\int_0^{+\infty}dk_\perp k_\perp\times\int_0^{k_\perp c}d\omega\,\mathrm{Re}\left[\frac{(r^\parallel_{sp})^2e^{-2k_\perp D}}{(1-r^2_{ss}e^{-2k_\perp D})(1-r^2_{pp}e^{-2k_\perp D})}\right], \tag{6a}$$

$$\Delta\mathcal{E}^\parallel_2\approx\frac{-\hbar}{4\pi^2}\int_0^{+\infty}dk_\perp k_\perp\int_0^{k_\perp c}d\omega\,\mathrm{Re}\left[\frac{\Delta r^2_{pp}e^{-2k_\perp D}}{(1-r^2_{pp}e^{-2k_\perp D})^2}\right], \tag{6b}$$

$$\Delta\mathcal{F}^\parallel_1\approx\frac{\hbar}{\pi^2}\int_0^{+\infty}dk_\perp k_\perp^2\times\int_0^{k_\perp c}d\omega\,\mathrm{Re}\left[\frac{(r^\parallel_{sp})^2[1-r^2_{ss}r^2_{pp}e^{-4k_\perp D}]e^{-2k_\perp D}}{([1-r^2_{ss}e^{-2k_\perp D}][1-r^2_{pp}e^{-2k_\perp D}])^2}\right], \tag{6c}$$

$$\Delta\mathcal{F}^\parallel_2\approx\frac{-\hbar}{2\pi^2}\int_0^{+\infty}dk_\perp k_\perp^2\times\int_0^{k_\perp c}d\omega\,\mathrm{Re}\left[\frac{\Delta r^2_{pp}(1+r^2_{pp}e^{-2k_\perp D})e^{-2k_\perp D}}{(1-r^2_{pp}e^{-2k_\perp D})^3}\right]. \tag{6d}$$

Of course, $\Delta\mathcal{E}^\parallel=\Delta\mathcal{E}^\parallel_1+\Delta\mathcal{E}^\parallel_2$ and $\Delta\mathcal{F}^\parallel=\Delta\mathcal{F}^\parallel_1+\Delta\mathcal{F}^\parallel_2$. For two different mirrors, the squares of the reflection coefficients have to be replaced as mentioned above. The integration over the angle φ is already performed. The reflection coefficients in Eq. (6) are given in Ref. [5]:

$$r_{sp}^{\parallel}(i\omega,ik_\perp)=-r_{ps}^{\parallel}(i\omega,ik_\perp)$$
$$=(-1)\frac{\sqrt{\omega^2-(k_\perp c)^2}\,\omega\,\varepsilon_{xy}(i\omega)(k_\perp c)}{(k_\perp c+\xi)[\varepsilon_{xx}(i\omega)k_\perp c+\xi]\xi}, \tag{7a}$$

$$\Delta r_{pp}(i\omega,ik_\perp)=\frac{2\sqrt{\omega^2-(k_\perp c)^2}\varepsilon_{xy}(i\omega)(k_\perp c)}{[\varepsilon_{xx}(i\omega)k_\perp c+\xi]^2}, \tag{7b}$$

again with $\xi=\sqrt{\omega^2[\varepsilon_{xx}(i\omega)-1]+(k_\perp c)^2}$. $r_{ss}(i\omega,ik_\perp)$ and $r_{pp}(i\omega,ik_\perp)$ are still given by Eq. (5a). Note that the contributions arising from the longitudinal and transversal Kerr effect are of opposite sign and therefore tend to cancel each other. On the basis of Eqs. (4)–(7), we will calculate the Casimir magnetic energies and forces for two simple models in the next two sections. In Sec. V, we will use these equations to numerically calculate the interaction for iron plates.

III. THE DRUDE MODEL

Consider two identical magnetic mirrors with a dielectric tensor described by the Drude model:

$$\varepsilon_{xx}(i\omega)=1+\frac{\omega_p^2\tau}{\omega(1+\omega\tau)}, \tag{8a}$$

$$\varepsilon_{xy}(i\omega)=\frac{\omega_p^2\omega_c\tau^2}{\omega(1+\omega\tau)^2}. \tag{8b}$$

In this equation, ω_p is the plasma frequency defined by $\omega_p \equiv 4\pi ne^2/m^\star$; ω_c is the cyclotron frequency given by $\omega_c \equiv eB_{\rm eff}/m^\star c$, where $B_{\rm eff}$ is the effective magnetic field experienced by the conduction electrons as a result of exchange and spin-orbit interactions; and τ is the relaxation time. In the usual situation, $\omega_c\tau \ll 1 \ll \omega_p\tau$.

There are three important distance regimes to consider. In the long-distance limit ($D \gg c\tau$) the dominant part in the integrals in Eqs. (4) and (6) comes from the region $\omega \leqslant k_\perp c \approx c/D \ll 1/\tau$. In this range, one has

$$\varepsilon_{xx}(i\omega)\approx\varepsilon_{xx}(i\omega)-1\approx\frac{\omega_p^2\tau}{\omega}\gg 1, \tag{9a}$$

$$\varepsilon_{xy}(i\omega)\approx\frac{\omega_p^2\omega_c\tau^2}{\omega}. \tag{9b}$$

With these approximations, one finds for the reflection coefficients:

$$r_{ss}(i\omega,ik_\perp)\approx -r_{pp}(i\omega,ik_\perp)\approx -1, \tag{10a}$$

$$r_{sp}^{\perp}(i\omega,ik_\perp)\approx -\frac{\omega_c}{\omega_p}\sqrt{\omega\tau}, \tag{10b}$$

$$r_{sp}^{\parallel}(i\omega,ik_\perp)\approx -\frac{\omega_c}{\omega_p^2}\sqrt{\omega^2-(k_\perp c)^2}, \tag{10c}$$

$$\Delta r_{pp}(i\omega,ik_\perp)\approx\frac{2\omega_c}{\omega_p^2}\frac{\omega\sqrt{\omega^2-(k_\perp c)^2}}{k_\perp c}. \tag{10d}$$

For the polar configuration, we arrive at

$$\Delta\mathcal{E}^{\perp}\approx -\frac{3\zeta(3)}{16\pi^2}\frac{\omega_c^2\tau}{\omega_p^2}\frac{\hbar c^2}{D^4}, \tag{11a}$$

$$\Delta\mathcal{F}^{\perp}\approx -\frac{3\zeta(3)}{4\pi^2}\frac{\omega_c^2\tau}{\omega_p^2}\frac{\hbar c^2}{D^5}. \tag{11b}$$

While for the in-plane configuration, it is found that

$$\Delta\mathcal{E}_1^{\parallel}\approx -\frac{\zeta(4)}{4\pi^2}\frac{\omega_c^2}{\omega_p^4}\frac{\hbar c^3}{D^5},\quad \Delta\mathcal{E}_2^{\parallel}\approx\frac{\zeta(4)}{10\pi^2}\frac{\omega_c^2}{\omega_p^4}\frac{\hbar c^3}{D^5}, \tag{12a}$$

$$\Delta\mathcal{E}^{\parallel}=\Delta\mathcal{E}_1^{\parallel}+\Delta\mathcal{E}_2^{\parallel}\approx -\frac{3\zeta(4)}{20\pi^2}\frac{\omega_c^2}{\omega_p^4}\frac{\hbar c^3}{D^5}, \tag{12b}$$

$$\Delta\mathcal{F}_1^{\parallel}\approx -\frac{5\zeta(4)}{4\pi^2}\frac{\omega_c^2}{\omega_p^4}\frac{\hbar c^3}{D^6},\quad \Delta\mathcal{F}_2^{\parallel}\approx\frac{\zeta(4)}{2\pi^2}\frac{\omega_c^2}{\omega_p^4}\frac{\hbar c^3}{D^6}, \tag{12c}$$

$$\Delta\mathcal{F}^{\parallel}=\Delta\mathcal{F}_1^{\parallel}+\Delta\mathcal{F}_2^{\parallel}\approx -\frac{3\zeta(4)}{4\pi^2}\frac{\omega_c^2}{\omega_p^4}\frac{\hbar c^3}{D^6}. \tag{12d}$$

The second regime is that for intermediate distances ($c/\omega_p \ll D \ll c\tau$). Now the integrals in Eqs. (4) and (6) are dominated by the range $1/\tau \ll \omega \leqslant k_\perp c \approx c/D \ll \omega_p$. For the elements of the dielectric tensor, one then finds

$$\varepsilon_{xx}(i\omega)\approx\varepsilon_{xx}(i\omega)-1\approx\frac{\omega_p^2}{\omega^2}\gg 1, \tag{13a}$$

$$\varepsilon_{xy}(i\omega)\approx\frac{\omega_p^2\omega_c}{\omega^3}. \tag{13b}$$

In this case, the reflection coefficients r_{ss}, r_{pp}, $r_{sp}^{\parallel}$, and Δr_{pp} still satisfy Eqs. (10a)–(10d), while

$$r_{sp}^{\perp}\approx -\frac{\omega_c}{\omega_p}. \tag{14}$$

Since the reflection coefficients for the in-plane configuration in this regime are not different from the ones in the short-distance limit, the expressions (12) are still valid for the Casimir magnetic energies and forces in the in-plane configuration. However, for the polar configuration, one has

$$\Delta\mathcal{E}^{\perp}\approx -\frac{1}{24}\frac{\hbar c}{D^3}\frac{\omega_c^2}{\omega_p^2}, \tag{15a}$$

$$\Delta\mathcal{F}^{\perp}\approx-\frac{1}{8}\frac{\hbar c}{D^4}\frac{\omega_c^2}{\omega_p^2}. \tag{15b}$$

The third regime to be considered is the limit of short distances ($D\ll c/\omega_p$). Here one has to distinguish between two regions: (i) $\omega\leqslant k_\perp c\ll\omega_p$ and (ii) $\omega_p\ll\omega\leqslant k_\perp c$. In region (i), the dielectric tensor elements are given in Eqs. (13), so the reflection coefficients $r_{sp}^{\perp}$, $r_{sp}^{\parallel}$, and Δr_{pp} are the same as those in the intermediate distance regime, but we will now make an expansion for r_{ss} and r_{pp} around -1 and 1, respectively,

$$r_{ss}(i\omega,ik_\perp)\approx-1+\frac{2k_\perp c}{\omega_p},\quad r_{pp}(i\omega,ik_\perp)\approx1-2\frac{\omega^2}{\omega_p k_\perp c}. \tag{16}$$

In region (ii), the dielectric tensor elements are given by

$$\varepsilon_{xx}(i\omega)-1\approx\frac{\omega_p^2}{\omega^2}\ll1, \tag{17a}$$

$$\varepsilon_{xy}(i\omega)\approx\frac{\omega_p^2\omega_c}{\omega^3}. \tag{17b}$$

We then find for region (ii),

$$r_{ss}(i\omega,ik_\perp)\approx0,\quad r_{pp}(i\omega,ik_\perp)\approx\frac{\omega_p^2}{2\omega^2+\omega_p^2}, \tag{18a}$$

$$r_{sp}^{\perp}(i\omega,ik_\perp)\approx-\frac{\omega_p^2\omega_c}{2}\frac{1}{(k_\perp c)(2\omega^2+\omega_p^2)}, \tag{18b}$$

$$r_{sp}^{\parallel}(i\omega,ik_\perp)\approx-\frac{\omega_p^2\omega_c}{2}\frac{\sqrt{\omega^2-(k_\perp c)^2}}{(k_\perp c)^2(2\omega^2+\omega_p^2)}, \tag{18c}$$

$$\Delta r_{pp}(i\omega,ik_\perp)\approx2\omega_p^2\omega_c\frac{\omega\sqrt{\omega^2-(k_\perp c)^2}}{(k_\perp c)(2\omega^2+\omega_p^2)^2}. \tag{18d}$$

With these approximations for the reflection coefficients in regions (i) and (ii), one finds the following expressions for the energies and forces (only the dominant term is given):

$$\Delta\mathcal{E}^{\perp}\approx-\frac{1}{16\sqrt{2}\pi}\omega_c^2\sqrt{\omega_p}\frac{\hbar}{c^{3/2}D^{1/2}}, \tag{19a}$$

$$\Delta\mathcal{F}^{\perp}\approx-\frac{1}{32\sqrt{2}\pi}\omega_c^2\sqrt{\omega_p}\frac{\hbar}{c^{3/2}D^{3/2}}, \tag{19b}$$

$$\Delta\mathcal{E}_1^{\parallel}\approx-\frac{1}{96\sqrt{2}\pi}\omega_c^2\sqrt{\omega_p}\frac{\hbar}{c^{3/2}D^{1/2}}, \tag{19c}$$

$$\Delta\mathcal{F}_1^{\parallel}\approx-\frac{1}{192\sqrt{2}\pi}\omega_c^2\sqrt{\omega_p}\frac{\hbar}{c^{3/2}D^{3/2}}, \tag{19d}$$

$$\Delta\mathcal{E}_2^{\parallel}\approx\frac{1}{16\sqrt{2}\pi}\sum_{n=0}^{+\infty}\left[\frac{(4n+3)!!}{(n+1)(4n+6)!!}\right]\frac{\omega_c^2}{\omega_p}\frac{\hbar}{D^2}, \tag{19e}$$

$$\Delta\mathcal{F}_2^{\parallel}\approx\frac{1}{8\sqrt{2}\pi}\sum_{n=0}^{+\infty}\left[\frac{(4n+3)!!}{(n+1)(4n+6)!!}\right]\frac{\omega_c^2}{\omega_p}\frac{\hbar}{D^3}. \tag{19f}$$

From these expressions, it is obvious that $\Delta\mathcal{E}^{\parallel}\approx\Delta\mathcal{E}_2^{\parallel}$ and $\Delta\mathcal{F}^{\parallel}\approx\Delta\mathcal{F}_2^{\parallel}$ for distances small enough. Note that for the polar configuration, the exponent of the dependence with respect to D obtained here in the short-distance limit differs from the one obtained in Ref. [3]. This is due to the effect of multiple reflections, which were neglected in Ref. [3] in this regime. It is interesting to note that although the reflection coefficients are much smaller than 1 in this high-frequency limit, the effect of multiple reflections is so important that the analytical dependence with D is modified. This is a unique feature of the magnetic Casimir effect.

It is clear that in the polar configuration, the energies are always negative. For the in-plane configuration, however, $\Delta\mathcal{E}_2^{\parallel}$ is positive, while $\Delta\mathcal{E}_1^{\parallel}$ is negative, so the sign of the resulting energy $\Delta\mathcal{E}^{\parallel}=\Delta\mathcal{E}_1^{\parallel}+\Delta\mathcal{E}_2^{\parallel}$ will depend on the magnitude of these two terms in the different regimes. As a result, a change of sign of the interaction is observed; in the long and intermediate-distance regimes, the total energy $\Delta\mathcal{E}^{\parallel}$ is negative, while for short distances it is positive. So whether the magnetic Casimir interaction is negative or positive depends on the distance between the mirrors.

We numerically calculated Eqs. (4) and (6) and compared them to the analytical expressions derived above. Details of the numerical procedure will be given in Sec. V. The absolute values of the magnetic Casimir forces per unit area (both numerical and analytical results) for distances between 1 nm and 10 μm for the two configurations are plotted in Fig. 1. Since typically $\tau\approx10^{-13}$ s, the long-distance regime ($D\gg c\tau\approx10$ μm) will not be visible in these plots. For the plots, a Drude model is used with $\hbar\omega_c=5.9$ meV and $\hbar\omega_p=9.85$ eV. As expected from the analytical results, the force in the in-plane configuration will be larger than that for the polar configuration for small enough distances ($D<10$ nm). The discontinuity at $D\approx40$ nm in the plot of the in-plane case depicts the change of sign. The analytical results are in pretty good agreement with the numerical calculations.

IV. THE HYBRID MODEL

The Drude model is not very realistic. Although it describes rather well the diagonal part of the dielectric tensor (except of course for the effect of interband transitions, which are not very important here), the off-diagonal part of the dielectric tensor is poorly described. This is because the latter is dominated by interband transitions. We therefore introduce a model (called ''hybrid model'') in which ε_{xx} is described by a plasma model,

$$\varepsilon_{xx}(i\omega)=1+\frac{\omega_p^2}{\omega^2}, \tag{20}$$

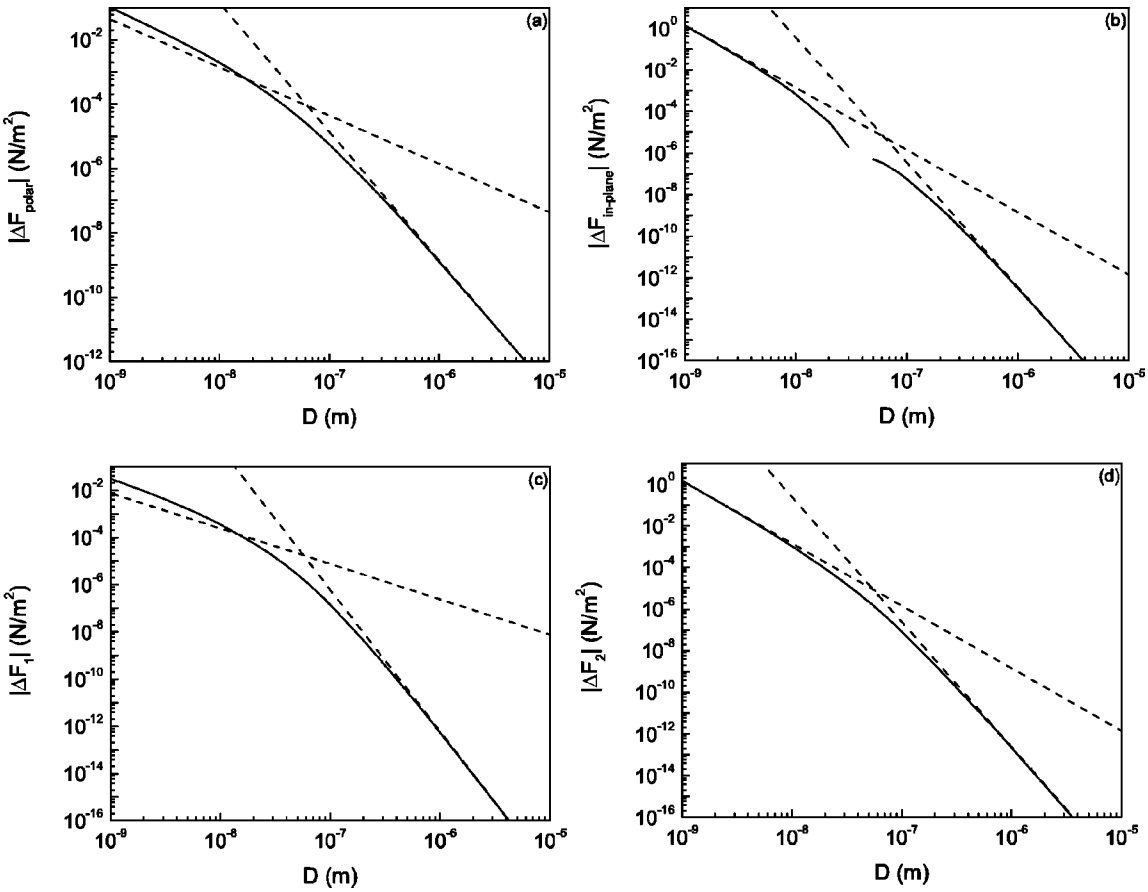

FIG. 1. Absolute values of the magnetic Casimir force (per unit area) with the mirrors described by a Drude model. Numerical results (solid curves) are compared with the analytical expressions (dashed curves) for the polar configuration (a), the in-plane configuration (b), the term $\Delta\mathcal{F}_1^{\parallel}$ resulting from the longitudinal Kerr effect (c), and the term from the transversal Kerr effect $\Delta\mathcal{F}_1^{\parallel}$ (d).

and where ε_{xy} is described by a single absorption line interband transition:

$$\mathrm{Re}\varepsilon_{xy}(\omega)\approx\omega_0\varepsilon_{xy}^{\mathrm{eff}}\delta(\omega-\omega_0). \tag{21}$$

In real systems ω_0 will be of the same order of magnitude as ω_p. The off-diagonal element of the dielectric tensor at imaginary frequency can be obtained by the following Kramers-Krönig relation:

$$\varepsilon_{xy}(i\omega)=\frac{2}{\omega\pi}\int_0^{+\infty}d\omega'\frac{\omega'^2\mathrm{Re}\,\varepsilon_{xy}(\omega')}{\omega'^2+\omega^2}, \tag{22}$$

and in this way we arrive at

$$\varepsilon_{xy}(i\omega)=\frac{2}{\pi}\frac{\omega_0^3\varepsilon_{xy}^{\mathrm{eff}}}{\omega(\omega_0^2+\omega^2)}. \tag{23}$$

For this model, we will only have two different integration regimes; the long-distance ($D\gg c/\omega_p$) and the short-distance regime ($D\ll c/\omega_p$). In the long-distance regime, the integrals in Eqs. (4) and (6) will be dominated by the range $\omega\leqslant k_\perp c\ll\omega_p$. In this range, we can approximate the dielectric tensor by

$$\varepsilon_{xx}(i\omega)\approx\varepsilon_{xx}(i\omega)-1\approx\frac{\omega_p^2}{\omega^2}\gg 1, \tag{24a}$$

$$\varepsilon_{xy}(i\omega)\approx\frac{2}{\pi}\frac{\omega_0\varepsilon_{xy}^{\mathrm{eff}}}{\omega}. \tag{24b}$$

One then finds for the reflection coefficients

$$r_{ss}(i\omega,ik_\perp)\approx-1,\quad r_{pp}(i\omega,ik_\perp)\approx 1, \tag{25a}$$

$$r_{sp}^{\perp}(i\omega,ik_\perp)\approx-\frac{2}{\pi}\frac{\omega_0\varepsilon_{xy}^{\mathrm{eff}}}{\omega_p^3}\omega^2, \tag{25b}$$

$$r_{sp}^{\parallel}(i\omega,ik_\perp)\approx-\frac{2}{\pi}\frac{\omega_0\varepsilon_{xy}^{\mathrm{eff}}}{\omega_p^4}\sqrt{\omega^2-(k_\perp c)^2}\,\omega^2, \tag{25c}$$

$$\Delta r_{pp}(i\omega,ik_\perp)\approx\frac{4}{\pi}\frac{\omega_0\varepsilon_{xy}^{\mathrm{eff}}}{\omega_p^4}\frac{\sqrt{\omega^2-(k_\perp c)^2}\,\omega^3}{k_\perp c}. \tag{25d}$$

With these approximations, we obtain for the magnetic Casimir energies and forces (per unit area):

$$\Delta\mathcal{E}^{\perp}\approx-\frac{\pi^2}{210}\frac{\omega_0^2(\varepsilon_{xy}^{\rm eff})^2}{\omega_p^6}\frac{\hbar c^5}{D^7}, \tag{26a}$$

$$\Delta\mathcal{F}^{\perp}\approx-\frac{\pi^2}{30}\frac{\omega_0^2(\varepsilon_{xy}^{\rm eff})^2}{\omega_p^6}\frac{\hbar c^5}{D^8}, \tag{26b}$$

$$\Delta\mathcal{E}_1^{\parallel}\approx-\frac{\pi^4}{1050}\frac{\omega_0^2(\varepsilon_{xy}^{\rm eff})^2}{\omega_p^8}\frac{\hbar c^7}{D^9}, \tag{26c}$$

$$\Delta\mathcal{F}_1^{\parallel}\approx-\frac{9\pi^4}{1050}\frac{\omega_0^2(\varepsilon_{xy}^{\rm eff})^2}{\omega_p^8}\frac{\hbar c^7}{D^{10}}, \tag{26d}$$

$$\Delta\mathcal{E}_2^{\parallel}\approx\frac{\pi^4}{945}\frac{\omega_0^2(\varepsilon_{xy}^{\rm eff})^2}{\omega_p^8}\frac{\hbar c^7}{D^9}, \tag{26e}$$

$$\Delta\mathcal{F}_2^{\parallel}\approx\frac{\pi^4}{105}\frac{\omega_0^2(\varepsilon_{xy}^{\rm eff})^2}{\omega_p^8}\frac{\hbar c^7}{D^{10}}, \tag{26f}$$

$$\Delta\mathcal{E}^{\parallel}\approx\frac{\pi^4}{9450}\frac{\omega_0^2(\varepsilon_{xy}^{\rm eff})^2}{\omega_p^8}\frac{\hbar c^7}{D^9}, \tag{26g}$$

$$\Delta\mathcal{F}^{\parallel}\approx\frac{\pi^4}{1050}\frac{\omega_0^2(\varepsilon_{xy}^{\rm eff})^2}{\omega_p^8}\frac{\hbar c^7}{D^{10}}. \tag{26h}$$

As in the Drude model, the force in the polar configuration will be negative. However, the total force for the in-plane configuration will be positive for the hybrid model in this distance regime.

In the limit of short distances, one has to distinguish between three different integration ranges while performing the integrals in Eqs. (4) and (6): region (i) where $\omega\leqslant k_\perp c\ll\omega_p$, region (ii) $k_\perp c\gg\omega_p$, $\omega\ll\omega_p$ and region (iii) $k_\perp c\gg\omega_p$, $\omega\gg\omega_p$. In region (i), r_{ss} and r_{pp} are defined by Eq. (16), while $r_{sp}^{\perp}$, $r_{sp}^{\parallel}$, and Δr_{pp} are given by Eqs. (25b)–(25d). In regions (ii) and (iii), we will do the calculations without multiple reflections [i.e., we put $r_{ss}(i\omega,ik_\perp)=r_{pp}(i\omega,ik_\perp)\approx0$]. In region (ii), the dielectric tensor elements are given in Eqs. (24), and the magneto-optical reflection coefficients are given by

$$r_{sp}^{\perp}(i\omega,ik_\perp)\approx-\frac{1}{\pi}\omega_0\varepsilon_{xy}^{\rm eff}\frac{\omega^2}{(k_\perp c)(2\omega^2+\omega_p^2)}, \tag{27a}$$

$$r_{sp}^{\parallel}(i\omega,ik_\perp)\approx-\frac{1}{\pi}\omega_0\varepsilon_{xy}^{\rm eff}\frac{\sqrt{\omega^2-(k_\perp c)^2}\,\omega^2}{(k_\perp c)^2(2\omega^2+\omega_p^2)}, \tag{27b}$$

$$\Delta r_{pp}(i\omega,ik_\perp)\approx\frac{4}{\pi}\omega_0\varepsilon_{xy}^{\rm eff}\frac{\sqrt{\omega^2-(k_\perp c)^2}\,\omega^3}{(k_\perp c)(2\omega^2+\omega_p^2)^2}. \tag{27c}$$

In region (iii), the dielectric tensor can be approximated by

$$\varepsilon_{xx}(i\omega)-1\approx\frac{\omega_p^2}{\omega^2}\ll1, \tag{28a}$$

$$\varepsilon_{xy}(i\omega)\approx\frac{2}{\pi}\frac{\omega_0^3\varepsilon_{xy}^{\rm eff}}{\omega^3}. \tag{28b}$$

One then finds for the magneto-optical reflection coefficients in region (iii):

$$r_{sp}^{\perp}(i\omega,ik_\perp)\approx-\frac{1}{\pi}\omega_0^3\varepsilon_{xy}^{\rm eff}\frac{1}{(k_\perp c)(2\omega^2+\omega_p^2)}, \tag{29a}$$

$$r_{sp}^{\parallel}(i\omega,ik_\perp)\approx-\frac{1}{\pi}\omega_0^3\varepsilon_{xy}^{\rm eff}\frac{\sqrt{\omega^2-(k_\perp c)^2}}{(k_\perp c)^2(2\omega^2+\omega_p^2)}, \tag{29b}$$

$$\Delta r_{pp}(i\omega,ik_\perp)\approx\frac{4}{\pi}\omega_0^3\varepsilon_{xy}^{\rm eff}\frac{\sqrt{\omega^2-(k_\perp c)^2}\,\omega}{(k_\perp c)(2\omega^2+\omega_p^2)^2}. \tag{29c}$$

With these equations by hand, we made an interpolation for the reflection coefficients in regions (ii) and (iii). This makes the calculation of the integrals less labor intensive because we can calculate the two regions at the same time. We have put

$$r_{sp}^{\perp}(i\omega,ik_\perp)\approx-\frac{\omega_0^3\varepsilon_{xy}^{\rm eff}}{\pi}\frac{\omega^2}{(k_\perp c)(2\omega^2+\omega_p^2)(\omega^2+\omega_0^2)}, \tag{30a}$$

$$r_{sp}^{\parallel}(i\omega,ik_\perp)\approx-\frac{\omega_0^3\varepsilon_{xy}^{\rm eff}}{\pi}\frac{\sqrt{\omega^2-k_\perp c^2}\,\omega^2}{(k_\perp c)^2(2\omega^2+\omega_p^2)(\omega^2+\omega_0^2)}, \tag{30b}$$

$$\Delta r_{pp}(i\omega,ik_\perp)\approx\frac{4\omega_0^3\varepsilon_{xy}^{\rm eff}}{\pi}\frac{\sqrt{\omega^2-(k_\perp c)^2}\,\omega^3}{(k_\perp c)(2\omega^2+\omega_p^2)^2(\omega^2+\omega_0^2)}. \tag{30c}$$

With these expressions for the reflection coefficients, we are finally ready to calculate the magnetic Casimir energies and forces for the short-distance regime. The result is

$$\Delta\mathcal{E}^{\perp}\approx-\frac{1}{4\sqrt{2}\pi^3}\frac{\omega_0^6(\varepsilon_{xy}^{\rm eff})^2}{(\omega_p+\sqrt{2}\omega_0)^3}\frac{\hbar}{c^2}\ln\left(\frac{c}{\omega^\star D}\right), \tag{31a}$$

$$\Delta\mathcal{F}^{\perp}\approx-\frac{1}{4\sqrt{2}\pi^3}\frac{\omega_0^6(\varepsilon_{xy}^{\rm eff})^2}{(\omega_p+\sqrt{2}\omega_0)^3}\frac{\hbar}{c^2D}, \tag{31b}$$

$$\Delta\mathcal{E}_1^{\parallel}\approx-\frac{1}{8\sqrt{2}\pi^3}\frac{\omega_0^6(\varepsilon_{xy}^{\rm eff})^2}{(\omega_p+\sqrt{2}\omega_0)^3}\frac{\hbar}{c^2}\ln\left(\frac{c}{\omega^\star D}\right), \tag{31c}$$

$$\Delta\mathcal{F}_1^{\parallel}\approx-\frac{1}{8\sqrt{2}\pi^3}\frac{\omega_0^6(\varepsilon_{xy}^{\rm eff})^2}{(\omega_p+\sqrt{2}\omega_0)^3}\frac{\hbar}{c^2D}, \tag{31d}$$

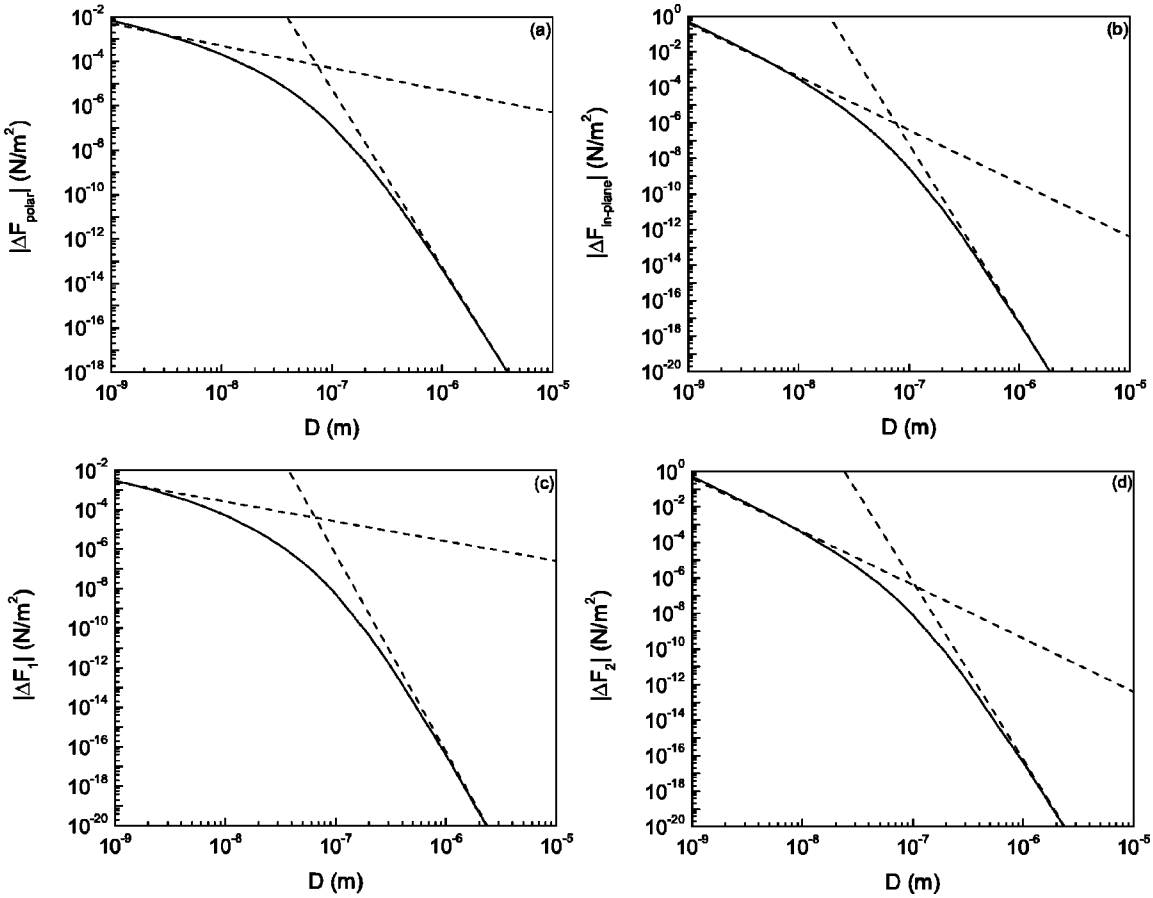

FIG. 2. Absolute values of the magnetic Casimir force (per unit area) with the mirrors described by the hybrid model. Numerical results (solid curves) are compared with the analytical expressions (dashed curves) for the polar configuration (a), the in-plane configuration (b), the term $\Delta\mathcal{F}_1^{\parallel}$ resulting from the longitudinal Kerr effect (c), and the term from the transversal Kerr effect $\Delta\mathcal{F}_1^{\parallel}$ (d).

$$\Delta\mathcal{E}_2^{\parallel}\approx\frac{1}{64\sqrt{2}\pi^3}\,\frac{\omega_0^6(\varepsilon_{xy}^{\mathrm{eff}})^2(\omega_p+5\sqrt{2}\omega_0)}{\omega_p(\omega_p+\sqrt{2}\omega_0)^5}\,\frac{\hbar}{D^2}, \quad (31e)$$

$$\Delta\mathcal{F}_2^{\parallel}\approx\frac{1}{32\sqrt{2}\pi^3}\,\frac{\omega_0^6(\varepsilon_{xy}^{\mathrm{eff}})^2(\omega_p+5\sqrt{2}\omega_0)}{\omega_p(\omega_p+\sqrt{2}\omega_0)^5}\,\frac{\hbar}{D^3}, \quad (31f)$$

with $\omega^\star$ a cutoff frequency of the order of the plasma frequency ω_p. It is clear that $\Delta\mathcal{E}^{\parallel}\approx\Delta\mathcal{E}_2^{\parallel}$ and $\Delta\mathcal{F}^{\parallel}\approx\Delta\mathcal{F}_2^{\parallel}$ for distances small enough. The force for the in-plane configuration is positive in this short-distance regime too, so there will not be a change of sign for this model.

We did the same numerical calculations as for the Drude model and compared the results with the analytical expressions in the different regimes. The following parameters were used in our hybrid model: $\hbar\omega_p=9.85$ eV, $\hbar\omega_0=3.9$ eV, $\varepsilon_{xy}^{\mathrm{eff}}=1.5\times10^{-2}$, and we have put $\omega^\star=2\exp(1)\omega_p$. In Fig. 2 the numerical and analytical results for the absolute value of the magnetic Casimir force are shown to be in rather good agreement.

V. NUMERICAL CALCULATIONS ON Fe

The Drude and hybrid model will not provide an accurate description for the dielectric tensor of the mirrors in a real system. This is because interband transitions will start playing a role at photon energies of a few eV, and these are not contained correctly in either of the models. In order to obtain an estimate of the magnitude of the magnetic Casimir force in such a real system, it is necessary to perform numerical calculations of Eqs. (4) and (6) where the reflection coefficients are calculated with experimental data for the dielectric tensor. In this section, we will present such calculations for a system with iron plates. Similar calculations for the nonmagnetic Casimir force have already been performed for Al, Au, and Cu [6,7].

Experimental values for the imaginary part of $\varepsilon_{xx}(\omega)$ for Fe are given in Ref. [8]. The diagonal element of the dielectric tensor at imaginary frequency can then be obtained by the causality relation

$$\varepsilon_{xx}(i\omega)=1+\frac{2}{\pi}\int_0^{+\infty}d\omega'\frac{\omega'\,\mathrm{Im}\,\varepsilon_{xx}(\omega')}{\omega'^2+\omega^2}. \quad (32)$$

Of course, it is impossible to perform the numerical integration over the entire interval $[0,+\infty]$, so we have to define our integration range in more detail. In our calculations, the complete range of data extending from 4 meV to 10 keV available in Ref. [8] was used, along with a Drude model below 4 meV, as shown in Fig. 3. The following parameters

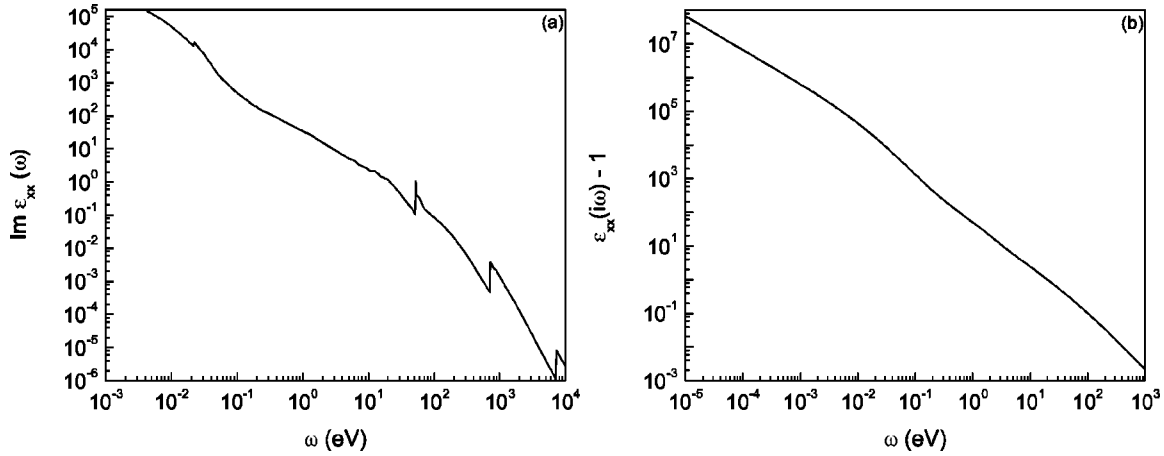

FIG. 3. The imaginary part of the diagonal element of the dielectric tensor evaluated at real frequencies (a) and the diagonal element as a function of imaginary frequency (b).

for the Drude model were found by extrapolation of the available data at low frequencies: $\hbar\omega_p = 3.5$ eV and $\hbar/\tau = 19$ meV. The quantity $\varepsilon_{xx}(i\omega) - 1$ calculated in this way is shown in Fig. 3 to decay roughly as $\omega^{-3/2}$ (for $\omega > \hbar/\tau$), so it cannot be completely described by a Drude (or plasma) model.

Experimental data for the off-diagonal element of the dielectric tensor is rather scarce. Some data for $\mathrm{Re}\,\varepsilon_{xy}(\omega)$ can be found in Ref. [9]. They are shown in Fig. 4. With the causality relation (22), it is then possible to calculate $\varepsilon_{xy}(i\omega)$. Since we only have data available between 0.1 eV and 6 eV, we had to perform the integration in Eq. (22) over this range. This, of course, is a rather rough approximation. The results of the calculation depicted in Fig. 4 show that $\varepsilon_{xy}(i\omega)$ decays the same way as in our hybrid model [cf. Eqs. (24b) and (27b)].

The magnetic Casimir force and energy are now calculated by numerical integration of Eqs. (4) and (6). We are interested in plate separations between 1 nm and 10 μm. These separations correspond to frequencies in the range 10^{-2}–10^{2} eV, so we will have to perform the integration between, say, 10^{-5} eV and 10^{4} eV. Figure 5 shows the resulting force and energy (per unit area) for the polar and in-plane configurations. In the short-distance limit, the force decays as D^{-2} for the polar configuration and as D^{-3} for the in-plane case. For long distances we find a D^{-6} power law for the polar configuration and D^{-8} for the situation with magnetization parallel to the plates. A change of sign of the interaction for the in-plane configuration is also visible from the figure (the discontinuity at $D = 50$ nm). The power laws differ (except for the in-plane configuration at short distances) from those obtained for the Drude and the hybrid model. This can be explained as due to the different behavior (because of interband transitions) of the dielectric tensor for Fe compared to that of the models. In view of future experimental investigations of the effect, distances $D > 10$ nm are the most interesting. In this range, the effect will be greatest for the polar configuration. For two parallel plates of Fe (with infinite lateral extension), the force per unit area in this configuration is approximately 40 mN/m^2 at $D = 10$ nm, and decays to 0.1 mN/m^2 at $D = 100$ nm. Whether such forces can be observed experimentally will be discussed in the following section.

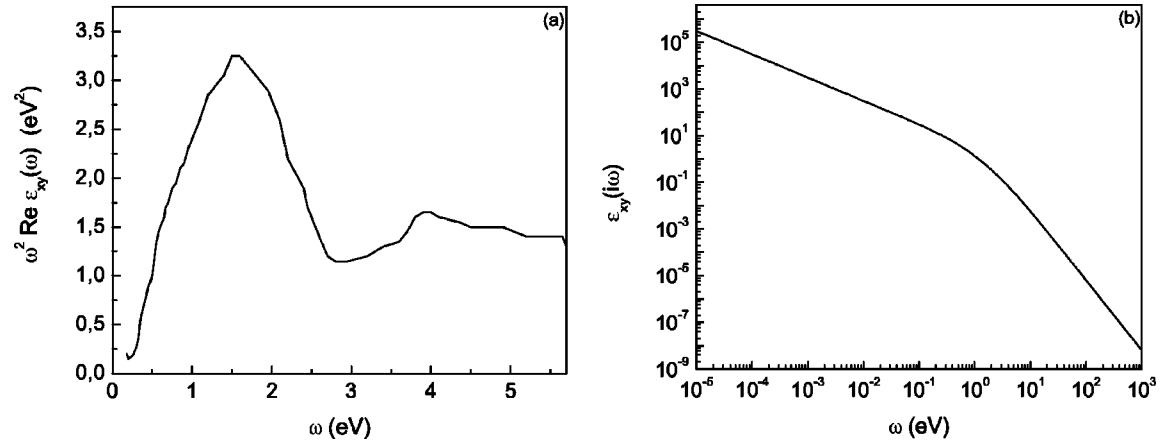

FIG. 4. The real part of the off-diagonal element of the dielectric tensor evaluated at real frequencies (multiplied by ω^2) (a) and the off-diagonal element as a function of imaginary frequency (b).

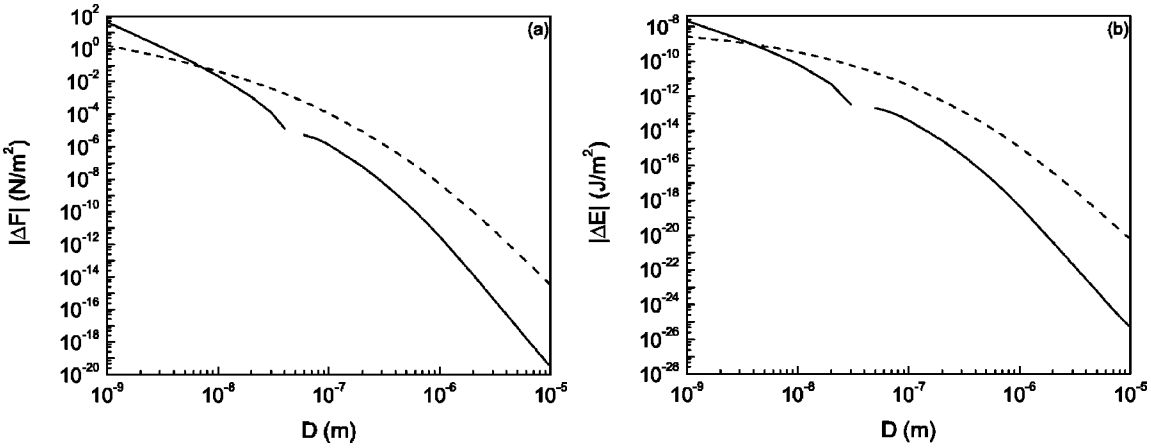

FIG. 5. Absolute values of the magnetic Casimir force per unit area (a) and the magnetic Casimir energy per unit area (b) between two iron plates (of infinite lateral extension). The solid curve corresponds to the in-plane configuration, while the dashed curve describes the polar configuration.

VI. EXPERIMENTAL SETUP

Since it is hard to experimentally maintain two parallel plates uniformly separated by distances smaller than a 1 μm, one of the plates is most often replaced by a lens-shaped mirror. Recently, a number of experiments has been performed using this geometry to measure the nonmagnetic Casimir force with an atomic force microscope [10–12]. For this plate-cylinder geometry, the Casimir force can be obtained from the plate-plate geometry by means of the force proximity theorem [13]:

$$\Delta F = 2\pi R\, \Delta \mathcal{E}(D). \tag{33}$$

In this equation, R is the radius of curvature of the lens-shaped mirror and $\Delta\mathcal{E}(D)$ is the Casimir energy per unit area for the configuration with two plates. One has to be careful to distinguish between ΔF and $\Delta\mathcal{F}$; the former is the force for the plate-lens geometry, while the latter is a force per unit area for two parallel plates. With the numerical results from the preceding section, we are able to estimate the magnitude of the magnetic Casimir force in the plate-lens geometry for Fe. If we take $R=100$ μm and a distance $D=50$ nm, a force $|\Delta F|\approx 10$ fN is found for the polar configuration. In the in-plane configuration, the force will be two orders of magnitude smaller. Such small forces can probably not be measured with the AFM technique. However, sensitivities of 0.1–10 fN in ''magnetic resonant force microscopy (MRFM)'' have been reported [14,15]. More recently, the detection of forces in the attonewton range has been achieved [16,17].

A possible MRFM setup is already discussed in detail in Ref. [3]. A thin film ($\approx$10 nm) of ferromagnetic material with hard magnetization is deposited on a substrate that is placed on a piezoelectric actuator. The lens-shaped mirror is attached to a cantilever by first depositing a small droplet of polymer on the cantilever, which can then be covered by evaporation with a thin ($\approx$10 nm) layer of soft ferromagnet (such as permalloy). In this way, one is able to create the lens shape, with a curvature radius of say 100 μm. The distance between the samples can be controlled easily with the piezo-actuator. By applying an ac magnetic field, one is able to modulate the magnetization of the soft sample at the resonance frequency of the cantilever. This will generate an oscillating magnetic Casimir force that causes the cantilever to vibrate. The deflection of the cantilever can then be measured with a laser. In this way, the magnetic force ($\Delta F = F_{AF} - F_{FM}$) can be measured. The force resolution achievable using a freely vibrating cantilever is fundamentally limited by intrinsic thermomechanical noise. This force noise can be controlled by the geometry of the cantilever; one needs a high-Q cantilever that is thin, narrow, and long to obtain the best sensitivity. With ultrathin silicon cantilevers, force resolutions in the attonewton range have been obtained [16]. More information on the sensitivity of MRFM can be found in Ref. [15,16].

Since the nonmagnetic Casimir effect is independent of the magnetization direction of the samples, only the magnetic contribution to the Casimir effect will be measured by using this modulation technique. Parasitic electrostatic forces (caused by a difference in potential between the magnetic samples) are also automatically taken care of in this way. The exchange interaction between the samples does not contribute much at the separations of interest ($D>10$ nm). Another parasitic magnetostatic interaction is the dipole interaction between the ferromagnets. This dipole force can be made as small as needed by taking a ferromagnetic plate with sufficiently large lateral extension and sufficiently small thickness. The plate should also be as uniformly magnetized as possible. With a plate of radius 1 cm and a thickness of 10 nm, this parasitic magnetostatic force can be estimated to be below 1 aN. Interaction of the soft sample with the ac magnetic field will yield a signal at two times the modulation frequency, so this can be filtered out effectively by using a lock-in amplifier. Thus with MRFM, it should be possible to measure the magnetic Casimir interaction without much influence of other effects.

VII. CONCLUSION

In this paper, the magnetic Casimir interaction discovered in Ref. [3] was generalized to the case where the magnetiza-

tion is parallel to the plates. The calculations for the Drude model in the short-distance limit were revised, and another model was introduced. The behavior of the interaction was discussed in the different distance regimes, and it is seen that the interaction in the two models decays quite differently with interplate distance. Numerical calculations for a real system with iron plates were also presented. Here we used experimental data for the dielectric tensor of the mirrors. The results from this numerical work on Fe could not be fitted by one of the introduced models, because interband transitions play a prominent role in Fe, and these were not implemented correctly in the models.

It was made acceptable that the new Casimir magnetic interaction can be measured with magnetic resonance force microscopy. However, to obtain an accurate comparison of the theory with eventual experimental results, more work is needed on the theoretical side. A detailed analysis of the geometrical effects would be valuable; the proximity force theorem does not provide reliable estimations at a level of accuracy of a few percent. Also, one has to consider other corrections already calculated for the nonmagnetic Casimir effect; e.g., surface roughness corrections would probably play an important role [18]. Finally, more experimental data on the off-diagonal element of the dielectric tensor for several ferromagnetic materials is also necessary in order to obtain a better estimate of the magnitude of the interaction from the numerical procedure presented.

[1] H.B.G. Casimir, Proc. K. Ned. Akad. Wet. **51**, 793 (1948).
[2] M. Bordag, U. Mohideen, and V.M. Mostepanenko, Phys. Rep. **353**, 1 (2001).
[3] P. Bruno, Phys. Rev. Lett. **88**, 240401 (2002).
[4] M.T. Jaekel and S. Reynaud, J. Phys. I **1**, 1395 (1991).
[5] G. Metzger, P. Pluvinage, and R. Torguet, Ann. Phys. (Paris) **10**, 5 (1965).
[6] S.K. Lamoreaux, Phys. Rev. A **59**, R3149 (1999).
[7] A. Lambrecht and S. Reynaud, Eur. Phys. J. D **8**, 309 (2000).
[8] *Handbook of Optical Constants of Solids*, edited by E. D. Palik (Academic Press, New York, 1991).
[9] *Numerical Data and Functional Relationships in Science and Technology*, Landolt-Börnstein, New Series Group, III Vol. 19, Pt. a (Springer, Berlin, 1992).
[10] U. Mohideen and A. Roy, Phys. Rev. Lett. **81**, 4549 (1998).
[11] A. Roy, C.-Y. Lin, and U. Mohideen, Phys. Rev. D **60**, 111101(R) (1999).
[12] B.W. Harris, F. Chen, and U. Mohideen, Phys. Rev. A **62**, 052109 (2000).
[13] J. Blocki, J. Randrup, W.J. Swiatecki, and C.F. Tsang, Ann. Phys. (N.Y.) **105**, 427 (1977).
[14] D. Rugar, O. Züger, S. Hoen, C.S. Yannoni, H.-M. Vieth, and R.D. Kendrick, Science **264**, 1560 (1994).
[15] J.A. Sidles, J.L. Garbini, K.J. Bruland, D. Rugar, O. Züger, S. Hoen, and C.S. Yannoni, Rev. Mod. Phys. **67**, 249 (1995).
[16] T.D. Stowe, K. Yasumura, T.W. Kenny, D. Botkin, K. Wago, and D. Rugar, Appl. Phys. Lett. **71**, 288 (1997).
[17] P. Mohanty, D.A. Harrington, and M.L. Roukes, Physica B **284-288**, 2143 (2000).
[18] A. Roy and U. Mohideen, Phys. Rev. Lett. **82**, 4380 (1999).